
Self-Supervised Implicit Attention: Guided Attention by The Model Itself

Jinyi Wu Xun Gong Zhemin Zhang
Southwest Jiaotong University
watson753@my.swjtu.edu.cn

Abstract

We propose **Self-Supervised Implicit Attention (SSIA)**, a new approach that adaptively guides deep neural network models to gain attention by exploiting the properties of the models themselves. SSIA is a novel attention mechanism that does not require any extra parameters, computation, or memory access costs during inference, which is in contrast to existing attention mechanism. In short, by considering attention weights as higher-level semantic information, we reconsidered the implementation of existing attention mechanisms and further propose generating supervisory signals from higher network layers to guide lower network layers for parameter updates. We achieved this by building a self-supervised learning task using the hierarchical features of the network itself, which **only** works at the training stage. To verify the effectiveness of SSIA, we performed a particular implementation (called an SSIA block) in convolutional neural network models and validated it on several image classification datasets. The experimental results show that an SSIA block can significantly improve the model performance, even outperforms many popular attention methods that require additional parameters and computation costs, such as Squeeze-and-Excitation and Convolutional Block Attention Module. Our implementation will be available on GitHub.

1 Introduction

In recent years, researchers have made many efforts to solve the problem of training very deep neural networks, such as designing better optimizers [46, 19], normalizing the initialization of model parameters [10, 13], using residual structures [14, 18], and so on. As these techniques have evolved, it has become possible to train very deep networks. These deep models, such as [34, 14, 5], have been proven to be powerful tools in various fields [23, 30, 2]; however, improving model performance by increasing the model parameters and computation is inefficient, and making models difficult to implement in practice. Therefore, self-attention methods that can improve model performance with fewer parameters and lower computation costs are becoming popular.

Existing attention methods proposed for convolutional neural network (CNN) models are typically designed as specialized modules, they inserted directly into the baseline CNN models to calculate attention weights along different dimensions of the feature maps [37, 17, 40, 16, 4, 39]. These calculated attention weights are believed to guide the baseline models to focus on *what* and *where*, which is **manually** applied to the input features to produce a refined feature map with element-wise multiplication, as in Squeeze-and-Excite (SE) [17] and Convolutional Block Attention Module (CBAM) [40], or addition, such as in the Non-local Neural Networks (NLN) [39] and Global Context Network (GCNet) [1]. These attention modules typically do not require additional supervision and are trained together with the baseline models to learn the distribution of the weights likely to identify useful features. We argue that these attention modules act on the feature maps explicitly and that their training is driven only by the weak supervisory signals generated from the top layer of the

network with task-related annotations (*e.g.*, category labels). We call this type of attention weakly supervised explicit attention. Such attention methods generally require additional parameters and computational costs. Although several attention methods requiring only a few (or even no) parameters or computational costs have been proposed recently [38, 42], they, as explicit attention, still require the inferring of attention weights and refining of feature maps. This increases the memory access and computational process, and hence reducing the inference speed.

In this paper, we proposed **Self-Supervised Implicit Attention (SSIA)** and its particular implementation, the SSIA block. SSIA is a fundamentally different attention mechanism that requires no additional parameters, computation, or memory access costs during inference. The core idea of implementing SSIA is to use the model’s intermediate feature maps to guide the attention of the model itself. By exploiting the inherent nature of deep neural networks during the training phase, supervisory signals, which guide parameter updates in the low network layers, are generated from the intermediate outputs of the networks. Since the SSIA implementation does **not** require refining feature maps explicitly but rather guides the baseline model to learn feature representations with better attentional properties during training, it does not need to calculate attention weights explicitly at the inference phase. In this aspect, SSIA seems to behave more like a regularization approach, such as weight decay [21] or dropout [33]. Probably the studies most closely related to ours are the recent works [24, 8, 22, 29] attempting to train attention modules through more direct supervised signals, such as extra annotation information [24] or reinforcement learning [22]. However, they still follow the idea of the mainstream explicit attention methods, which consider the attention module to be a specialized module functionally separated from the baseline model and implement attention by manually refining feature maps. In contrast, our SSIA builds self-supervised learning tasks from the baseline model itself by leveraging the *feature hierarchical nature* [47, 43, 11], and gives the low layer features better attention properties by learning. Because SSIA does not work by explicitly modifying feature maps, we argue that it imposes *implicit* attention on baseline models.

In summary, our main contributions are as follows:

1. We reconsidered the implementation of existing attention mechanisms in deep learning models and propose a self-supervised attention training technique. The result is SSIA, a novel attention mechanism.
2. We designed a novel attention module, the SSIA block, to implement the proposed SSIA mechanism on computer vision tasks and study its advantages.
3. We validate the SSIA block on several classification datasets, which showed that it significantly improves the model performance without requiring extra parameters, computation, or memory access costs during inference.

2 Method

2.1 Motivation

Fundamentally, we know that the essence of attention mechanism is the perception of global-level information and its use in the assignment of computational weights. Thus, the models with attention can retain more task-relevant valuable information at a (relatively) more global level in the low-to-high forward-propagation process. We considered this definition of attention and made the following two observations:

- *First*, we observed that previous attention approaches [17, 40, 1, 27, 38, 42] could be generally divided into three steps: (1) modeling the context of the input features to generate global descriptors, (2) performing nonlinear transformations on global descriptors to generate attention weights, (3) refining the input feature maps by applying these attention weights. The pipeline is shown in Figure 1a. We argue that these attention methods actually perform the perception of global-level information in Steps 1 and 2, and perform the assignment of computational weights in Step 3.
- *Second*, according to previous studies [47, 43], features learned by deep convolutional neural networks (DCNNs) have a self-organized and hierarchical feature representation, that is, a *hierarchical-feature nature* [11]. This means that DCNN models produce feature maps with higher-level semantic representations at the higher network layers (in both spatial and channel dimensions), which naturally have a more global-level perception than lower network layers.

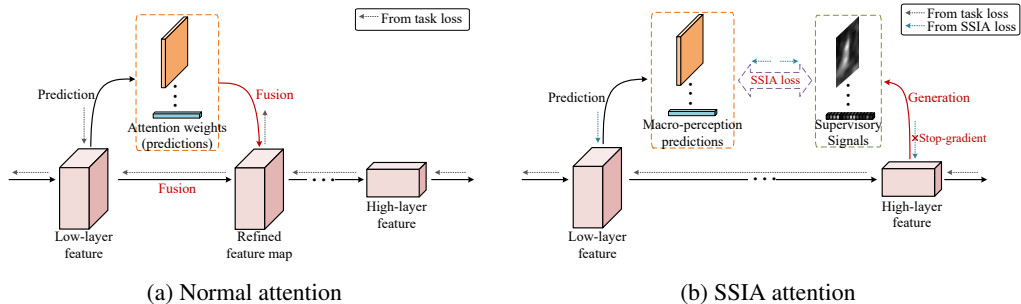


Figure 1: Comparison on SSIA attention and other attention methods. (a) is generalized "explicit" attention, which implements attention by refining feature maps, and (b) is our "implicit" SSIA, which is guided by the built self-supervised task losses. The red color is used in the figures to highlight their differences. The gray dashed arrows indicate the top-down gradient flow of the target task loss, and the blue dashed arrows indicate the gradient flow of the SSIA loss.

Combining these two observations, we reexamined previous implementations of the attention mechanism and concluded that the three-steps process, as shown in Figure 1a, is **not** necessary — it is not necessary to generate attention weights explicitly and assign computational weights *manually*. Attention can also be implemented in a neural network model if the original low-layer features can acquire the perception of global-level information (denoted as macro-perception) through the training process, allowing subsequent network layers to perform *adaptive* assignment of computational weights. Combined with the hierarchical-feature nature of CNNs, we posed an intuitive question: can low network layers benefit from the natural macro-perception of higher network layers during training, thus guiding the model to gain attention?

Based on the above idea, we devised our novel attention mechanism, SSIA, and built a particular implementation called the SSIA block for typical CNN models. As shown in Figure 1b, the SSIA block attempts to build a self-supervised learning task that enables the features learned in lower network layers to predict higher-level features using a weak predictor and penalizing prediction failures. To reduce the prediction error, the trained low network layers tend to produce features with more high-level semantic properties, which the subsequent network layers can use. The SSIA block can be discarded after training, whereas the SSIA attention is implemented in the model.

2.2 SSIA Block

SSIA is implemented on CNNs by a computational unit called an SSIA block, which is plugged into the baseline model during the training phase. Each SSIA block accepts two different layers of feature maps as input and yields an auxiliary self-supervised loss. Specifically, each SSIA block contains three main parts: (i) a *weak predictor*, the macro-perception predictor (MPP), which predicts the macro-perception information that the input low-layer features should have when they forward-propagate to the higher layers, (ii) an untrainable *supervisory signal generator*, which uses high-layer features to generate supervisory signals, and (iii) an *SSIA loss* which measures the deviation of the predictions.

The workflow of an SSIA block is shown in Figure 2. These three components work together to guide the MPP and low network layers in updating. For simplicity, we denote the input side of the MPP in the SSIA block as the *prediction side* and the input side of the supervisory signal generator as the *signal side*. The backward gradients are only passed at the prediction side and stop gradients at the signal side.

Since MPP is a **weak** predictor, it is inherently limited in its capability. Therefore, to reduce the self-supervised loss introduced by the SSIA block during back-propagation, the network tends to learn feature representations that have significant macro-perception semantics so that the weak MPP can easily use this information to make good predictions. Finally, the network outputs intermediate feature maps with better macro-perception information (*i.e.*, better attentional properties), which the higher layers can further use.

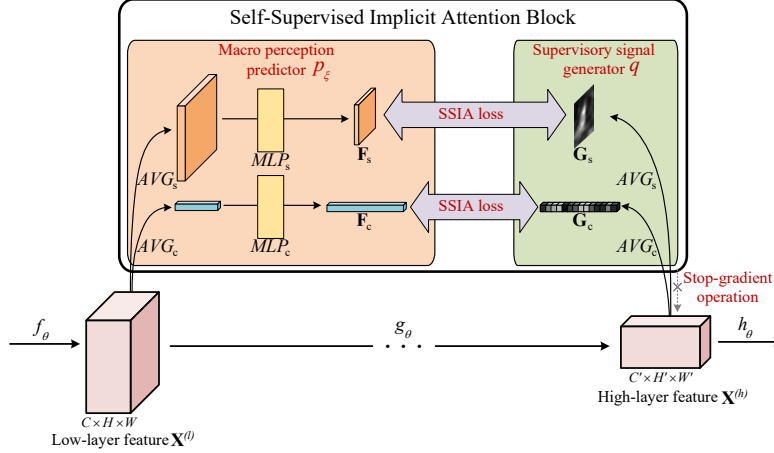


Figure 2: SSIA block architecture. It’s a particular implementation of SSIA on CNNs, it takes feature maps of two different depth layers as inputs to generate macro-perception predictions and supervisory signals, respectively, then computes SSIA losses in spatial and channel dimensions.

More formally, let the input of the baseline model be I , forward-propagated on the network to obtain the l -th layer feature map $\mathbf{X}^{(l)} \in \mathbb{R}^{C \times H \times W}$, which can be summarized as $\mathbf{X}^{(l)} = f_{\theta}(I)$. Then, $\mathbf{X}^{(l)}$ continues to forward-propagate to the h -th layer feature map $\mathbf{X}^{(h)} \in \mathbb{R}^{C' \times H' \times W'}$, this process can be summarized as $\mathbf{X}^{(h)} = g_{\theta}(\mathbf{X}^{(l)})$. We feed $\mathbf{X}^{(l)}$ and $\mathbf{X}^{(h)}$ into the prediction side and the signal side, respectively, of an SSIA block. Due to the hierarchical-feature nature of the neural network, the high-layer feature map $\mathbf{X}^{(h)}$ finds information on a more global level than the lower-layer feature map $\mathbf{X}^{(l)}$. Using these notational conventions, we describe the details of each part of our SSIA block implementation in the following.

Supervisory Signal Generator. To guide low network layers with high-level features, the supervisory signal generator takes the high-layer feature map $\mathbf{X}^{(h)}$ as input and generates different types of the supervisory signals $\mathbf{G}_1, \mathbf{G}_2, \dots, \mathbf{G}_m$. These supervisory signals can be considered as the descriptions of different aspects of the macro-perception information, which the high-layer feature map $\mathbf{X}^{(h)}$ naturally has. This process can be expressed as $\mathbf{G}_1, \mathbf{G}_2, \dots, \mathbf{G}_m = q(\mathbf{X}^{(h)})$, where $q(\cdot)$ denotes the supervisory signal generator, and $\mathbf{G}_1, \mathbf{G}_2, \dots, \mathbf{G}_m$ depend on the types of implicit attention to be imposed. We only generate spatial supervisory signal $\mathbf{G}_s \in \mathbb{R}^{1 \times H' \times W'}$ and channel supervisory signal $\mathbf{G}_c \in \mathbb{R}^{C' \times 1 \times 1}$ of the high-layer feature map $\mathbf{X}^{(h)}$.

In our SSIA block implementation, $q(\cdot)$ first generates the spatial and channel global descriptors by using global pooling operations, then normalize them in the corresponding dimensions to obtain \mathbf{G}_s and \mathbf{G}_c . This is more formally expressed as:

$$\mathbf{G}_s = \text{Norm}(\text{AVG}_s(\mathbf{X}^{(h)})), \quad (1)$$

$$\mathbf{G}_c = \text{Norm}(\text{AVG}_c(\mathbf{X}^{(h)})), \quad (2)$$

where $\text{Norm}(\cdot)$ denotes the normalization operation applied to tensors (*i.e.*, subtract their mean and divide the variance). AVG_s and AVG_c denote global average pooling operations along the spatial and channel dimensions, respectively.

Macro-Perception Predictor. The MPP takes the low-level feature $\mathbf{X}^{(l)}$ of an image as input and makes predictions $\mathbf{F}_1, \mathbf{F}_2, \dots, \mathbf{F}_m$ about the macro-perception information it propagates to the high-level feature map $\mathbf{X}^{(h)}$. This process can be expressed as $\mathbf{F}_1, \mathbf{F}_2, \dots, \mathbf{F}_m = p_{\xi}(\mathbf{X}^{(l)})$, where p_{ξ} denotes the weak predictor MPP with the trainable parameters ξ . The predicted macro-perception information, $\mathbf{F}_1, \mathbf{F}_2, \dots, \mathbf{F}_m$, corresponds to the supervisory signals $\mathbf{G}_1, \mathbf{G}_2, \dots, \mathbf{G}_m$. Therefore, we only predict the macro-perception information $\mathbf{F}_s \in \mathbb{R}^{1 \times H' \times W'}$ and $\mathbf{F}_c \in \mathbb{R}^{C' \times 1 \times 1}$ related to the spatial and channel dimensions, respectively, with the same tensor sizes as the supervisory signals

\mathbf{G}_s and \mathbf{G}_c . The predictions \mathbf{F}_s and \mathbf{F}_c are analogous to the spatial attention (maps) and channel attention (vectors) in existing attention methods (e.g., CBAM [40] and BAM [27]), which we call spatial macro-perception prediction and channel macro-perception prediction.

In our SSIA block implementation, \mathbf{F}_s and \mathbf{F}_c are computed as follows: 1) obtain the spatial descriptor ϕ_s and channel descriptor ϕ_c using global average pooling operations along different dimensions of the low-layer feature map $\mathbf{X}^{(l)}$ to aggregate statistical information, then 2) (optional) normalize ϕ_s and ϕ_c and scale the spatial descriptor to reduce the computational cost, and finally, 3) forward ϕ_s and ϕ_c to their respective multilayer perceptron (MLP) predictors to produce the macro-perception predictions \mathbf{F}_s and \mathbf{F}_c , respectively. The overall process can be expressed as follows:

$$\mathbf{F}_s = MLP_s(\phi_s) = MLP_s(AVG_s(\mathbf{X}^{(l)})), \quad (3)$$

$$\mathbf{F}_c = MLP_c(\phi_c) = MLP_c(AVG_c(\mathbf{X}^{(l)})), \quad (4)$$

where both MLP_s and MLP_c are MLPs with a single hidden layer (with a batch normalization layer). We compress the hidden layer size of MLP_s and MLP_c to a lower dimension to reduce their parameters and computational costs during training. Note that the formula description above ignores, for simplicity, the optional normalization of ϕ_s and ϕ_c and the scaling of ϕ_s . In practice, the spatial descriptor ϕ_s can be scaled by bilinear interpolation or local average pooling, which reduces the parameters and computational costs of MLP_s .

SSIA Loss. The total training loss is the weighted summation of the total SSIA loss, \mathcal{L}_{total}^{sb} , and the baseline model’s task loss, $\mathcal{L}_{total}^{task}$, more formally describe as $\mathcal{L} = \lambda^{task} \mathcal{L}_{total}^{task} + \lambda^{sb} \mathcal{L}_{total}^{sb}$, where λ^{task} and λ^{sb} are hyperparameters of the relative contribution of these two losses. The total SSIA loss generated by all N inserted SSIA blocks is \mathcal{L}_{total}^{sb} , which finally guides the model’s attention during the back-propagation process. It is calculated as follows:

$$\mathcal{L}_{total}^{sb} = \sum_{n=1}^N \lambda_n^{sb} \mathcal{L}^{sb}(\mathbf{X}^{(l_n)}, \mathbf{X}^{(h_n)}), \quad (5)$$

where $\mathcal{L}^{sb}(\mathbf{X}^{(l_n)}, \mathbf{X}^{(h_n)})$ denotes the self-supervised loss introduced by the n -th SSIA block, and $\mathbf{X}^{(l_n)}$ and $\mathbf{X}^{(h_n)}$ denote the input feature maps of the n -th SSIA block’s prediction and signal sides, respectively, which are the intermediate feature maps output from the baseline model. λ_n^{sb} is a hyperparameter indicating the relative contribution of the n -th SSIA block.

The loss of a single SSIA block is given by $\mathcal{L}^{sb}(\mathbf{X}^{(l_n)}, \mathbf{X}^{(h_n)}) = \sum_{i=1}^m \lambda_i^{ssia} \mathcal{L}^{ssia}(\mathbf{F}_i, sg(\mathbf{G}_i))$, where $sg(\cdot)$ denotes the stop-gradient operation, \mathcal{L}^{ssia} is the SSIA loss measure for each predicted macro-perception, and λ_i^{ssia} is the hyperparameter. We only use the supervisory signals in spatial and channel dimensions, so the self-supervised loss can be simplified to:

$$\mathcal{L}^{sb}(\mathbf{X}^{(l_n)}, \mathbf{X}^{(h_n)}) = \lambda_s \mathcal{L}^{ssia}(\mathbf{F}_s, \mathbf{G}_s) + \lambda_c \mathcal{L}^{ssia}(\mathbf{F}_c, \mathbf{G}_c). \quad (6)$$

The SSIA loss function \mathcal{L}^{ssia} measures the deviation between prediction results $\mathbf{F}_1, \mathbf{F}_2, \dots, \mathbf{F}_m = p_\xi(\mathbf{X}^{(l)})$ and their corresponding supervisory signals $\mathbf{G}_1, \mathbf{G}_2, \dots, \mathbf{G}_m = q(\mathbf{X}^{(h)})$. It is related to how the MPP prediction task is constructed. We constructed the MPP prediction task through regression to leverage the supervisory signals and guide the parameter updates. Thus, \mathcal{L}^{ssia} is calculated as follows:

$$\mathcal{L}^{ssia}(\mathbf{F}, \mathbf{G}) = \sum_k \frac{valid(\mathbf{G}(k))}{\varepsilon + \sum_k valid(\mathbf{G}(k))} \cdot (\mathbf{F}(k) - \mathbf{G}(k))^2, \quad (7)$$

where \mathbf{F} indicates the MPP macro-perception prediction result of (for us, \mathbf{F}_s and \mathbf{F}_c), and \mathbf{G} indicates the supervisory signal corresponding to it (for us, \mathbf{G}_s and \mathbf{G}_c). The variable k traverses all spatial locations when $\mathbf{G} = \mathbf{G}_s$; similarly, the variable k traverses all channels when $\mathbf{G} = \mathbf{G}_c$. ε is a small positive real number that serves to prevent division errors (e.g., $\varepsilon = 10^{-8}$). The function $valid(\cdot)$ is used to limit the supervisory signals to a specific intensity range. Specifically,

$$valid(\mathbf{G}(k)) = \mathbb{I}[|\mathbf{G}(k)| > \eta] \cdot \mathbb{I}[|\mathbf{G}(k)| < 10], \quad (8)$$

where $\mathbb{I}[\cdot]$ is an indicator function that takes the value 1 when the condition inside the square brackets is true and 0 otherwise. On the right side of the above equation, the first term ignores the effect of ambiguous supervisory signals (those close to 0), and the second term limits the intensity of valid supervisory signals to the range $(-10, 10)$, avoiding extreme loss values caused by outliers. η is the supervisory signal threshold for both positive and negative feature activation.

For convenience, we refer to the implicit attention imposed by the SSIA loss in the spatial (using \mathbf{F}_s and \mathbf{G}_s) and channel (using \mathbf{F}_c and \mathbf{G}_c) dimensions as spatial SSIA and channel SSIA, respectively. Note that, although we used the same SSIA loss function, \mathcal{L}^{ssia} , for **all** types of macro-perception predictions, \mathbf{F}_i , for similarity, it is possible to design different SSIA losses for each.

3 Experiments

In this section, we first perform a series of ablation experiments on the classification task over the mini-ImageNet dataset [36] to prove the effectiveness of our proposed SSIA and analyze the design choices of the SSIA block. Next, we compare the performance to that of other state-of-the-art attention methods on the CIFAR datasets [20] and ImageNet-1K dataset [30]. Finally, we perform a visual analysis of the baseline model trained with the SSIA block. To evaluate the performance of the SSIA block fairly, all our experiments were implemented in the PyTorch framework [28] with the same backbone, ResNet [14], as the baseline model. For other attention modules, we use the hyperparameter settings in their papers.

3.1 Implement Details

It is worth noting that the primary purpose of our experiments was to validate the effectiveness of the SSIA as an attention mechanism, not to find the specific best-performing implementation of an SSIA block. Moreover, the best hyperparameter settings and connection positions for the SSIA block may be different for specific tasks and baseline models. However, based on experimental experience, these minor differences in hyperparameter settings usually do **not** significantly influence the performance of the SSIA block. In fact, an appropriately placed SSIA block nearly always works on any baseline model. Therefore, unless otherwise noted, the hyperparameters and prediction side placement described below were used for the SSIA block in all the experiments.

Regarding connecting the SSIA block in the baseline model, both the prediction side and signal side of the SSIA block can receive any size of feature maps as input, so, **theoretically**, it can be plugged into any position in a model. For example, with the typical ResNet [14] as the baseline model, we created only three SSIA blocks, and we plugged the output feature maps of stages 1-3 into their prediction side, while the output feature maps of each stage were plugged into their signal sides. As the example shown in Figure 3, each SSIA block takes the output feature maps of the next stage of its prediction side location as the signal side inputs.

Regarding the hyperparameters settings, we used the same settings for all inserted SSIA blocks. Specifically, to reduce the parameters and computational costs, we set the bottleneck layer size to $d = 64$ and applied bilinear interpolation to reduce the size of the spatial descriptors (if needed). Note that different downsampling approaches may lead to slightly different results. The hyperparameters that control the relative contributions of spatial and channel SSIA losses are $\lambda_s = 1$ and $\lambda_c = 3$; the positive/negative example threshold is $\eta = 0.5$. The relative contribution coefficients are $\lambda_1^{sb} = 1$, $\lambda_2^{sb} = 2$, and $\lambda_3^{sb} = 3$ (numbering from the lowest layer to highest layer), and the contribution ratios between the total SSIA loss and the classification task loss are $\lambda^{task} = 1$ and $\lambda^{sb} = 0.2$.

All models in our experiments followed the standard training pipeline. Specifically, the 224×224 image used for training was a randomly scaled cropped version of the original image or its horizontal mirror image. During the evaluation, it was a centrally cropped 224×224 image after scaling the shortest edge of the image to 256 pixels (preserving the aspect ratio). We used a stochastic gradient descent (SGD) optimizer with a momentum of 0.9 and a weight decay factor of $4e-5$, the learning rate starting from 0.1 with cosine descent as in [15]. Without extra declaration, all networks were trained on a single GPU with a mini-batch size of 32 and 100 epochs totally.

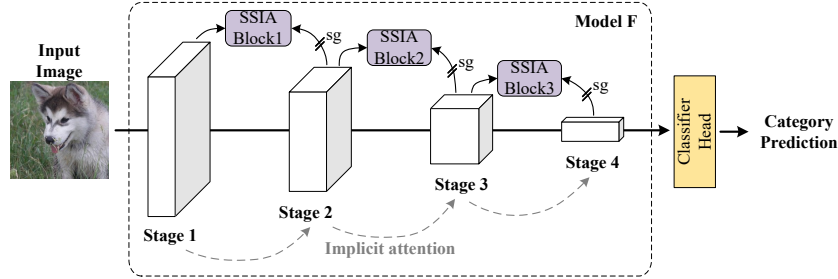


Figure 3: SSIA block integrated with a general ResNet model. As illustrated, we plugged the SSIA block into each two adjacent stages, where the feature map of the lower stage is used as the prediction side and the feature map of the higher stage is used as the signal side. "sg" means stop-gradient operation. The direction of the guided attention is indicated by the dashed gray arrow.

3.2 Ablation Studies

In this subsection, we used ResNet-50 [14] as the baseline model and performed ablation experiments over the mini-ImageNet [36] dataset. The hyperparameters settings and connection positions of the SSIA blocks were the same as described above unless otherwise specified. Mini-ImageNet is a subset of the ImageNet dataset, which contains 60,000 images in 100 categories, with 600 images per category. The original mini-ImageNet dataset is used for few-shot learning [36] with different training and testing categories. We reintegrated it into a classification task dataset, took 20% of the images from each category as the validation set, and used the remaining images as the training set. The classification accuracy reported is for the validation set.

Spatial SSIA vs. Channel SSIA. We experimentally verified that both channel SSIA and spatial SSIA could effectively improve model performance. Table 1 shows their comparative results, where "Ch." or/and "Sp." indicates the type of SSIA imposed (Channel or/and Spatial). These experiments used the same hyperparameters settings and training pipeline except that, when only spatial SSIA was used, we set $\lambda_s = 1$ and $\lambda_c = 0$; when only channel SSIA was used, we set $\lambda_s = 0$ and $\lambda_c = 3$; when both were used, we set $\lambda_s = 0.5$ and $\lambda_c = 1.5$.

The experimental results show that SSIA in both the spatial and channel dimensions can significantly improve the accuracy of the baseline model, and their combination further improves the accuracy. This suggests that the attention guided by different supervisory signals has different properties: they appear to guide different aspects of the global-level perceptibility of the baseline models. Therefore, we use spatial SSIA and channel SSIA simultaneously in all subsequent experiments.

Signal Side Selection. As previously described, the SSIA block can use the feature maps of any layer as the signal side input and produce supervisory signals, we experimentally compare the impact of this difference in choice on performance. Intuitively, the higher the feature map is, the more semantic (and more global-level) information it contains, but also the more difficult it is to predict from low-layer features. Because there are too many options for choosing the signal side location, we only show several representative schemes, each SSIA block is connected to the signal side with: (i)

Table 1: Top-1 and Top-5 accuracies (%) for the ResNet-50 baseline model with different variants of the SSIA block on mini-ImageNet.

Model	Top-1	Top-5
ResNet50 (baseline)	79.59	93.45
+ SSIA Ch.	81.54	94.62
+ SSIA Sp.	81.97	94.67
+ SSIA Ch. & Sp.	82.31	94.65

Table 2: Top-1 and Top-5 accuracies (%) for different signal side choice schemes of the SSIA block on mini-ImageNet.

Model	Top-1	Top-5
ResNet50 (baseline)	79.59	93.45
+ final SSIA	82.19	94.61
+ cascaded SSIA	82.31	94.65
+ identity SSIA	80.23	94.11

Table 3: Comparisons between different attention modules and our SSIA block, with ResNet-50 as the baseline. Includes the top-1 accuracies (%) on the CIFAR-10 (C10), CIFAR-100 (C100) and ImageNet-1K (ImageNet) datasets, the increments in parameters (+Params), computation (+FLOPs), and memory usage (+MUs) compared to the baseline model. These baseline model costs shown in the table are for the backbone network (with no classifier head).

Model	C10	C100	ImageNet	+Params	+FLOPs	+MUs
ResNet50 (baseline)	93.63	74.45	76.21	(23.51M)	(4.116G)	(109.68M)
+ SE	95.35	77.25	76.98	2.52M	0.009G	0.12M
+ CBAM	95.37	77.67	77.21	2.53M	0.012G	0.4M
+ BAM	94.86	77.28	77.07	0.36M	0.091G	3.05M
+ ECA	94.55	76.16	76.75	86	0.006G	0.18M
+ SimAM	95.65	78.42	76.91	0	0.001G	21.06M
+ SSIA block	95.69	78.59	77.13	0	0	0

the output feature maps of the last stage, (ii) the output feature maps of the next stage of its prediction side location (Figure 3), and (iii) the output feature maps of the same location as the prediction side. In this experiment, the selection of the prediction sides and other settings were kept the same. In addition, we scaled the spatial supervisory signals of connected SSIA blocks to 28×28 , 14×14 , and 7×7 (from low to high) in all schemes for a fair comparison. The experimental results are shown in Table 2, where the final SSIA, cascade SSIA, and identity SSIA correspond to schemes (i), (ii), and (iii) described above, respectively.

The experimental results show that scheme (ii) is the best choice, followed by scheme (i). While scheme (iii), which uses the same layer feature maps as the signal side, performed significantly poorer than the other schemes because it does not introduce any more global-level perceptual information than the prediction side. In fact, our further studies proved that the unexpected improvement of scheme (iii) came from some unexpected regularization effects of SSIA loss in the initial training stage. To eliminate this phenomenon just ignore the SSIA loss in the first few iterations of training. It also proves that the guidance of macro-perception information (in higher layer feature maps) to the lower network layers was the main reason for the performance improvement. Therefore, we use scheme (ii) for the choice of signal sides in all subsequent experiments.

3.3 Image Classification

In this subsection, we compare the performance of the SSIA block to that of other attention methods used in CNNs on the CIFAR datasets [20] and ImageNet dataset [30], including the widely used SE [17], CBAM [40], and BAM [27]; we also compare them to the lightweight attention methods efficient channel attention (ECA) [38] and SimAM [42]. Note that on ImageNet-1K dataset, the performance of our SSIA block was related to the batch size (see the Appendix for details), we report the results with a batch size of 64. The attention methods we compared were trained under the same settings. As shown in Table 3, our implicit attention module, the SSIA block, significantly improved the performance of the baseline model, it takes $\sim 4.2\%$ accuracy improvement on the CIFAR-100 dataset, even surpassing all other explicit attention methods. On ImageNet-1K dataset, SSIA block also effectively improves model performance (by nearly 1% accuracy improvement) and outperforms most of the state-of-the-art attention methods we compared.

Besides achieving a considerable performance improvement, the SSIA block has the following two additional advantages: (1) it generates more substantial and direct supervisory signals to guide attention by building self-supervised learning tasks without designing complex procedures or requiring additional manual annotation, and (2) it works entirely during the training phase and does not introduce any parameters, computation, or memory access costs at the inference phase.

Since many attention modules are designed to be very lightweight with few additional parameters and computational costs (such as ECA and SimAM), the second advantage of SSIA block may not seem obvious. However, in practice, an explicit attention method always introduces branching structures, they introduce a much larger inference time cost than intuitively we think. How branching structures affect the inference speed of a model has been discussed in detail in recent works (*e.g.*, RepVGG [6]) that attempt to eliminate branching structures in networks.

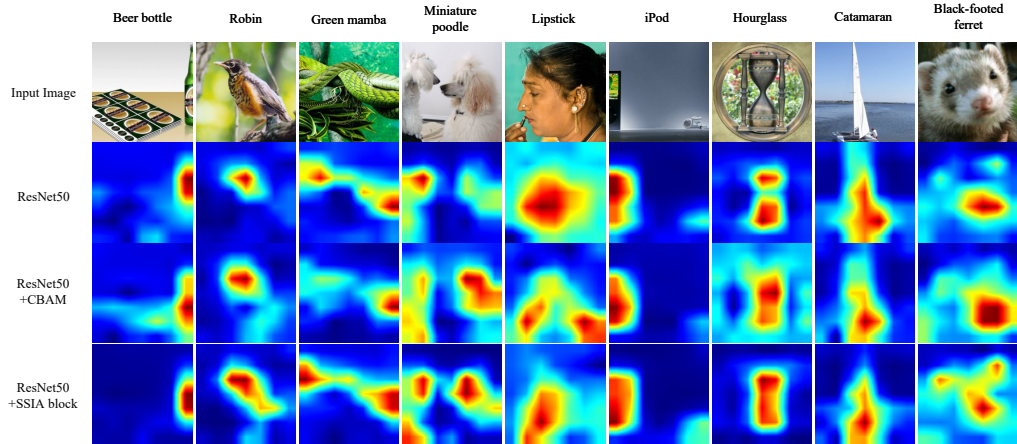


Figure 4: CAM visualization results. This visualization compares the CAM [49] for ResNet-50 trained with vanilla, CBAM [40], and our SSIA block. The CAM visualization is calculated for the last convolutional layer outputs.

3.4 Visualization Results

To verify whether the SSIA block helped the baseline model acquire better attentional capabilities, we used class activation mapping (CAM) [49] to visualize the results. As shown in Figure 4, the CAM activation of the SSIA-block-integrated model produced more significant attentional properties than the vanilla model.

It can be seen in most cases that the model integrated with the SSIA block more effectively suppressed the background and covered a more complete area of the main object regions, which indicates that the model has better attentional properties. Because the SSIA block does not work during inference, we argue that these benefits are due to the SSIA block guiding the baseline model to obtain explicit attention (*i.e.*, the SSIA attention) during training. Moreover, this suggests that specialized attention modules are **not** a necessary component for implementing attention mechanisms.

4 Conclusion

In this paper, we review the implementation of existing attention mechanisms and propose SSIA, a novel implementation paradigm for attention mechanism. We further explore a particular implementation, called the SSIA block, for implementing SSIA in CNN models. The SSIA block plugged into the baseline model can simply be discarded after the training phase, so it does not introduce any costs during the inference phase. Our experimental results showed that the SSIA block works well in visual classification tasks and is very competitive with other well-known explicit attention methods used in CNNs. Our visualization results proved that the baseline model integrated with an SSIA block has better attentional properties. In future work, we plan to investigate various SSIA implementations and use them in other computer-vision tasks. To the best of our knowledge, this paper is the first to propose the use of implicit attention instead of explicit attention. We hope that our work will inspire new studies on the attention methods used in deep-learning models.

References

- [1] Yue Cao, Jiarui Xu, Stephen Lin, Fangyun Wei, and Han Hu. Gcnet: Non-local networks meet squeeze-excitation networks and beyond. *2019 IEEE/CVF International Conference on Computer Vision Workshop (ICCVW)*, pages 1971–1980, 2019.
- [2] Liang-Chieh Chen, George Papandreou, Iasonas Kokkinos, Kevin P. Murphy, and Alan Loddon Yuille. Deeplab: Semantic image segmentation with deep convolutional nets, atrous convolution, and fully connected crfs. *IEEE Transactions on Pattern Analysis and Machine Intelligence*, 40:834–848, 2018.

- [3] Xinlei Chen and Kaiming He. Exploring simple siamese representation learning. *2021 IEEE/CVF Conference on Computer Vision and Pattern Recognition (CVPR)*, pages 15745–15753, 2021.
- [4] Yunpeng Chen, Yannis Kalantidis, Jianshu Li, Shuicheng Yan, and Jiashi Feng. A2-nets: Double attention networks. In *NeurIPS*, 2018.
- [5] François Chollet. Xception: Deep learning with depthwise separable convolutions. *2017 IEEE Conference on Computer Vision and Pattern Recognition (CVPR)*, pages 1800–1807, 2017.
- [6] Xiaohan Ding, X. Zhang, Ningning Ma, Jungong Han, Guiguang Ding, and Jian Sun. Repvgg: Making vgg-style convnets great again. *2021 IEEE/CVF Conference on Computer Vision and Pattern Recognition (CVPR)*, pages 13728–13737, 2021.
- [7] Jeff Donahue, Philipp Krähenbühl, and Trevor Darrell. Adversarial feature learning. *ArXiv*, abs/1605.09782, 2017.
- [8] Hiroshi Fukui, Tsubasa Hirakawa, Takayoshi Yamashita, and Hironobu Fujiyoshi. Attention branch network: Learning of attention mechanism for visual explanation. *2019 IEEE/CVF Conference on Computer Vision and Pattern Recognition (CVPR)*, pages 10697–10706, 2019.
- [9] Spyros Gidaris, Praveer Singh, and Nikos Komodakis. Unsupervised representation learning by predicting image rotations. *ArXiv*, abs/1803.07728, 2018.
- [10] Xavier Glorot and Yoshua Bengio. Understanding the difficulty of training deep feedforward neural networks. In *AISTATS*, 2010.
- [11] Ian J. Goodfellow, Yoshua Bengio, and Aaron C. Courville. Deep learning. *Nature*, 521:436–444, 2015.
- [12] Jean-Bastien Grill, Florian Strub, Florent Althé, Corentin Tallec, Pierre H. Richemond, Elena Buchatskaya, Carl Doersch, Bernardo Ávila Pires, Zhaohan Daniel Guo, Mohammad Gheshlaghi Azar, Bilal Piot, Koray Kavukcuoglu, Rémi Munos, and Michal Valko. Bootstrap your own latent: A new approach to self-supervised learning. *ArXiv*, abs/2006.07733, 2020.
- [13] Kaiming He, X. Zhang, Shaoqing Ren, and Jian Sun. Delving deep into rectifiers: Surpassing human-level performance on imagenet classification. *2015 IEEE International Conference on Computer Vision (ICCV)*, pages 1026–1034, 2015.
- [14] Kaiming He, X. Zhang, Shaoqing Ren, and Jian Sun. Deep residual learning for image recognition. *2016 IEEE Conference on Computer Vision and Pattern Recognition (CVPR)*, pages 770–778, 2016.
- [15] Tong He, Zhi Zhang, Hang Zhang, Zhongyue Zhang, Junyuan Xie, and Mu Li. Bag of tricks for image classification with convolutional neural networks. *2019 IEEE/CVF Conference on Computer Vision and Pattern Recognition (CVPR)*, pages 558–567, 2019.
- [16] Jie Hu, Li Shen, Samuel Albanie, Gang Sun, and Andrea Vedaldi. Gather-excite: Exploiting feature context in convolutional neural networks. In *NeurIPS*, 2018.
- [17] Jie Hu, Li Shen, and Gang Sun. Squeeze-and-excitation networks. *2018 IEEE/CVF Conference on Computer Vision and Pattern Recognition*, pages 7132–7141, 2018.
- [18] Gao Huang, Zhuang Liu, and Kilian Q. Weinberger. Densely connected convolutional networks. *2017 IEEE Conference on Computer Vision and Pattern Recognition (CVPR)*, pages 2261–2269, 2017.
- [19] Diederik P. Kingma and Jimmy Ba. Adam: A method for stochastic optimization. *CoRR*, abs/1412.6980, 2015.
- [20] Alex Krizhevsky. Learning multiple layers of features from tiny images. In *Technical report, University of Toronto*, 2009.
- [21] Anders Krogh and John A. Hertz. A simple weight decay can improve generalization. In *NIPS*, 1991.
- [22] Duo Li and Qifeng Chen. Deep reinforced attention learning for quality-aware visual recognition. In *ECCV*, 2020.
- [23] Tsung-Yi Lin, Michael Maire, Serge J. Belongie, James Hays, Pietro Perona, Deva Ramanan, Piotr Dollár, and C. Lawrence Zitnick. Microsoft coco: Common objects in context. In *ECCV*, 2014.
- [24] Drew Linsley, Dan Shiebler, Sven Eberhardt, and Thomas Serre. Learning what and where to attend. In *ICLR*, 2019.

- [25] Mehdi Noroozi and Paolo Favaro. Unsupervised learning of visual representations by solving jigsaw puzzles. In *ECCV*, 2016.
- [26] Mehdi Noroozi, Hamed Pirsiavash, and Paolo Favaro. Representation learning by learning to count. *2017 IEEE International Conference on Computer Vision (ICCV)*, pages 5899–5907, 2017.
- [27] Jongchan Park, Sanghyun Woo, Joon-Young Lee, and In So Kweon. A simple and light-weight attention module for convolutional neural networks. *International Journal of Computer Vision*, 128:783–798, 2020.
- [28] Adam Paszke, Sam Gross, Francisco Massa, Adam Lerer, James Bradbury, Gregory Chanan, Trevor Killeen, Zeming Lin, Natalia Gimelshein, Luca Antiga, Alban Desmaison, Andreas Köpf, Edward Yang, Zach DeVito, Martin Raison, Alykhan Tejani, Sasank Chilamkurthy, Benoit Steiner, Lu Fang, Junjie Bai, and Soumith Chintala. Pytorch: An imperative style, high-performance deep learning library. In *NeurIPS*, 2019.
- [29] Badri N. Patro and Vinay P. Namboodiri. Self supervision for attention networks. *2021 IEEE Winter Conference on Applications of Computer Vision (WACV)*, pages 726–735, 2021.
- [30] Olga Russakovsky, Jia Deng, Hao Su, Jonathan Krause, Sanjeev Satheesh, Sean Ma, Zhiheng Huang, Andrej Karpathy, Aditya Khosla, Michael S. Bernstein, Alexander C. Berg, and Li Fei-Fei. Imagenet large scale visual recognition challenge. *International Journal of Computer Vision*, 115:211–252, 2015.
- [31] Mark Sandler, Andrew G. Howard, Menglong Zhu, Andrey Zhmoginov, and Liang-Chieh Chen. Mobilenetv2: Inverted residuals and linear bottlenecks. *2018 IEEE/CVF Conference on Computer Vision and Pattern Recognition*, pages 4510–4520, 2018.
- [32] Karen Simonyan and Andrew Zisserman. Very deep convolutional networks for large-scale image recognition. *CoRR*, abs/1409.1556, 2015.
- [33] Nitish Srivastava, Geoffrey E. Hinton, Alex Krizhevsky, Ilya Sutskever, and Ruslan Salakhutdinov. Dropout: a simple way to prevent neural networks from overfitting. *J. Mach. Learn. Res.*, 15:1929–1958, 2014.
- [34] Christian Szegedy, Vincent Vanhoucke, Sergey Ioffe, Jonathon Shlens, and Zbigniew Wojna. Rethinking the inception architecture for computer vision. *2016 IEEE Conference on Computer Vision and Pattern Recognition (CVPR)*, pages 2818–2826, 2016.
- [35] Pascal Vincent, H. Larochelle, Isabelle Lajoie, Yoshua Bengio, and Pierre-Antoine Manzagol. Stacked denoising autoencoders: Learning useful representations in a deep network with a local denoising criterion. *J. Mach. Learn. Res.*, 11:3371–3408, 2010.
- [36] Oriol Vinyals, Charles Blundell, Timothy P. Lillicrap, Koray Kavukcuoglu, and Daan Wierstra. Matching networks for one shot learning. In *NIPS*, 2016.
- [37] Fei Wang, Mengqing Jiang, Chen Qian, Shuo Yang, Cheng Li, Honggang Zhang, Xiaogang Wang, and Xiaoou Tang. Residual attention network for image classification. *2017 IEEE Conference on Computer Vision and Pattern Recognition (CVPR)*, pages 6450–6458, 2017.
- [38] Qilong Wang, Banggu Wu, Pengfei Zhu, P. Li, Wangmeng Zuo, and Qinghua Hu. Eca-net: Efficient channel attention for deep convolutional neural networks. *2020 IEEE/CVF Conference on Computer Vision and Pattern Recognition (CVPR)*, pages 11531–11539, 2020.
- [39] X. Wang, Ross B. Girshick, Abhinav Kumar Gupta, and Kaiming He. Non-local neural networks. *2018 IEEE/CVF Conference on Computer Vision and Pattern Recognition*, pages 7794–7803, 2018.
- [40] Sanghyun Woo, Jongchan Park, Joon-Young Lee, and In-So Kweon. Cbam: Convolutional block attention module. In *ECCV*, 2018.
- [41] Saining Xie, Ross B. Girshick, Piotr Dollár, Zhuowen Tu, and Kaiming He. Aggregated residual transformations for deep neural networks. *2017 IEEE Conference on Computer Vision and Pattern Recognition (CVPR)*, pages 5987–5995, 2017.
- [42] Lingxiao Yang, Ru-Yuan Zhang, Lida Li, and Xiaohua Xie. Simam: A simple, parameter-free attention module for convolutional neural networks. In *ICML*, 2021.
- [43] Jason Yosinski, Jeff Clune, Anh M Nguyen, Thomas J. Fuchs, and Hod Lipson. Understanding neural networks through deep visualization. *ArXiv*, abs/1506.06579, 2015.
- [44] Sergey Zagoruyko and Nikos Komodakis. Wide residual networks. *ArXiv*, abs/1605.07146, 2016.

- [45] Jure Zbontar, Li Jing, Ishan Misra, Yann LeCun, and Stéphane Deny. Barlow twins: Self-supervised learning via redundancy reduction. In *ICML*, 2021.
- [46] Matthew D. Zeiler. Adadelata: An adaptive learning rate method. *ArXiv*, abs/1212.5701, 2012.
- [47] Matthew D. Zeiler and Rob Fergus. Visualizing and understanding convolutional networks. In *ECCV*, 2014.
- [48] Xiangyu Zhang, Xinyu Zhou, Mengxiao Lin, and Jian Sun. Shufflenet: An extremely efficient convolutional neural network for mobile devices. *2018 IEEE/CVF Conference on Computer Vision and Pattern Recognition*, pages 6848–6856, 2018.
- [49] Bolei Zhou, Aditya Khosla, Àgata Lapedriza, Aude Oliva, and Antonio Torralba. Learning deep features for discriminative localization. *2016 IEEE Conference on Computer Vision and Pattern Recognition (CVPR)*, pages 2921–2929, 2016.

A Appendix

MPP Prediction Results. We visualized the spatial perception prediction results of the trained MPP, as shown in Figure 5. It can be seen that the macro-perception predictions of the SSIA block exhibit strong target and background discrimination capabilities, with some even made at low network layers. With existing attention methods such as BAM, whose prediction results are also shown in Figure 5), it is difficult to distinguish the main object and background semantically in the predicted attention maps because these methods are guided only by weakly supervised signals. The attention maps predicted by the BAM block appear to discriminate the saliency of regions based on texture features, especially in the lower layers of the network.

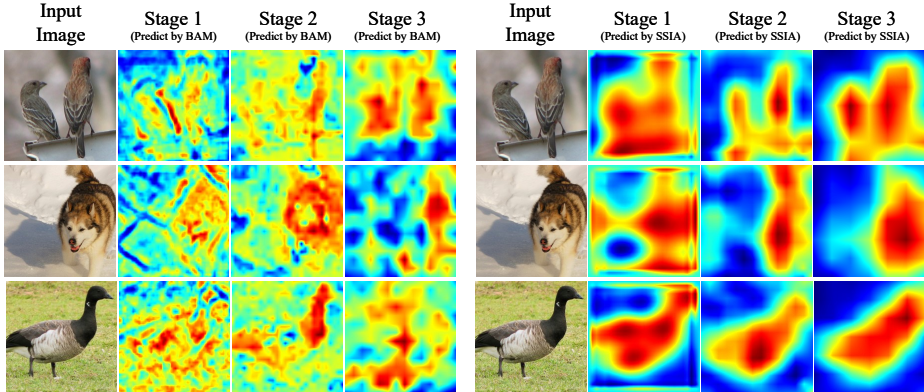


Figure 5: SSIA block and BAM predicted outputs. This visualization used the trained ResNet-50 model with either an integrated SSIA block or BAM [27]. The columns from left to right are the input images, the spatial macro-perception predictions (or the spatial attention map predictions) of either the SSIA block or BAM connected at stages 1-3. For the comparison, the results were post-processed and converted to heat maps.

Because these results were output as intermediate results in the forward-propagation process, a trained MPP could predict global-level semantics directly from the current layer feature maps, comparable to that of high-layer feature maps. These by-products of the SSIA block may be useful for other computer-vision tasks or approaches.

Relationship to Contrastive Learning. Self-supervised learning is a sub-branch of representation learning, which aims to mine supervisory information from large-scale unlabeled data by pretext tasks [35, 25, 26, 9, 7] and train the network with that supervised information to learn representations that are useful for the target task. Consider the SSIA block as a self-supervised learning strategy that is not designed to learn robust feature representations of images but to make the feature representations with better attentional properties (*i.e.*, SSIA). In fact, the core idea of implementing SSIA is to obtain supervisory signals by mining the intermediate feature representations of the *previous version* of the network rather than relying on annotation information. These supervisory signals serve as a target to guide the lower layers to perform parameter updates, producing the next version of the feature representations. That version of the feature representations can produce the next guide target in turn, and so forth. This process is very similar to some contrastive learning methods using twin networks, such as [12, 3, 45]. To further reveal the subtle relationship between SSIA and the contrastive learning paradigm, we have given the Siamese network form of the SSIA block and compared it with such contrastive learning methods in the following.

Figure 6a shows a simplified version of SimSiam [3], where the target network is a replicated version of the online network (an encoder) sharing the same model parameters. Two different augmented views of the same input image are formed as a pair of samples as input to the Siamese network, and a weak predictor (a MLP) predicts the output vector of the target network from the output vector of the online network. The output vector of the target network is used as supervisory signals with a stop-gradient operation, and the weak predictor and the baseline model are updated by back-propagation to maximize the similarity between the prediction results and the supervisory signals.

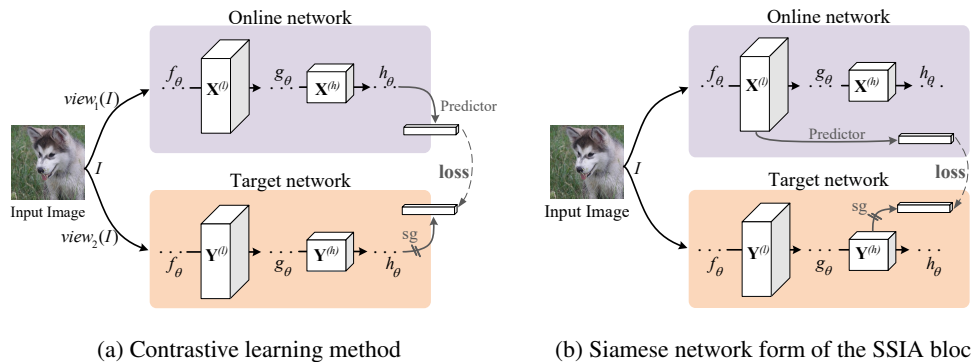


Figure 6: Comparison on the SSIA block and the contrastive learning paradigm. Where (a) is a simplified SimSiam architecture, and (b) is the siamese network form of the SSIA block, "sg" means stop-gradient operation. This figure mainly focuses on the process of generating losses from intermediate feature maps, and the network layers are not illustrated for simplicity (denoted by ellipsis dots and letters).

Table 4: Top-1 accuracy (%) for ResNet-50 in its vanilla version (baseline) and the SSIA-block-integrated version on ImageNet-1K dataset, with different batch size settings. Both spatial and channel SSIA was used for all SSIA block, with the cascaded connection scheme.

Model	batch size		
	64	128	256
ResNet50 (baseline)	76.21	76.17	76.28
+ SSIA block	77.13	76.93	76.41

Figure 6b shows our proposed SSIA implementation, the SSIA block, with its Siamese network form implementation, its workflow is nearly the same as the contrastive learning workflow in Figure 6a, except (1) the online and target networks of the SSIA block have the same input image, (2) the weak predictor generates macro-perception predictions from the intermediate feature map of the online network, and (3) the supervisory signals are generated from the intermediate feature map of the target network.

It can be seen that the SSIA learning process is similar to the representation learning process driven by contrastive learning methods, as both use the feature representations of the data from the previous version of the baseline model during training. Those features are used as supervisory signals for updating the model parameters in the next step. It appears that the SSIA block performs some type of representation learning for better attention properties through such a self-supervised paradigm.

Note that the Siamese network form is proposed only for the convenience of understanding how SSIA is related to contrastive learning methods, An SSIA block only forward-propagates once for each sample in practice (only the target network).

Image Classification on ImageNet-1K. On ImageNet-1K dataset, the effectiveness of SSIA block is related to the batch size. In general, the performance improvement brought from the SSIA block becomes weaker as the batch size increases, as shown in Table 4. Too large batch size (≥ 256) will lead to a weak effect of SSIA block.

We will investigate the reasons for this phenomenon and its countermeasures in future work. Nevertheless, the experiments still confirm that SSIA is an effective attention mechanism.

SSIA Block in Different CNN Backbones. We compared the performance of the vanilla version and the SSIA-block-integrated version of several popular CNN backbones in Table 5 on the mini-ImageNet [36] dataset, including VGG-16 [32], ResNet-18/50/101 [14], Wide ResNet-18 [44] and

Table 5: Top-1 and Top-5 accuracies (%) for different backbone models in their vanilla version and the integrated-SSIA-block version on the mini-ImageNet dataset. We use both spatial and channel SSIA with the cascaded connection scheme for all SSIA block.

Backbone	baseline models		with SSIA block	
	Top-1 acc.	Top-5 acc.	Top-1 acc.	Top-5 acc.
VGG16	73.39	90.88	74.41 (+1.02)	91.58 (+0.70)
ResNet18	78.32	92.85	80.19 (+1.87)	93.74 (+0.89)
ResNet50	79.59	93.45	82.31 (+2.72)	94.65 (+1.20)
ResNet101	80.57	94.04	82.86 (+2.29)	94.97 (+0.95)
WideResNet18 (widen=1.5)	78.78	93.16	81.03 (+2.25)	93.95 (+0.79)
WideResNet18 (widen=2.0)	79.58	93.49	81.60 (+2.02)	94.41 (+0.92)
ResNeXt50 (32x4d)	80.25	93.79	82.31 (+2.06)	94.76 (+0.97)
ResNeXt101 (32x4d)	81.28	94.36	82.90 (+1.62)	94.71 (+0.35)
MobileNetV2	78.18	93.81	78.82 (+0.64)	93.93 (+0.12)
ShuffleNetV2	78.33	93.59	78.97 (+0.64)	93.75 (+0.16)

ResNeXt-50/101 [41]. All the baseline models with the SSIA block significantly outperformed their vanilla versions, which suggests the proposed SSIA block can work well on various CNN backbones.

We also applied the SSIA block to the lightweight CNN networks, such as MobileNet [31] and ShuffleNet [48], as shown in Table 5. Their improvement is not as evident as on other backbone networks, so it appears that the SSIA block works especially well on typical CNN networks with residual connections. However, we found that the SSIA loss declined during training in lightweight networks (as in other networks), which implies that the lower network layers indeed learn features with better macro-perception information. This may hint us that some design within such lightweight networks influences the use of these features in higher network layers, such as depthwise separable convolutions.

The way to make SSIA attention work well on lightweight networks is a valuable topic for implementing deep-learning models in practice, which we intend to investigate in the future.